Pergamon

Int. J. Solids Structures Vol. 32, No. 1, pp. 89–103, 1995

0020-7683/95 $9.50 + .00

0020-7683(94)00109-X

QUASI-STATIC AND BALLISTIC PERFORATION OF CARBON FIBER LAMINATES

WERNER GOLDSMITH, C. K. H. DHARAN and HUI CHANG†
Department of Mechanical Engineering, University of California, Berkeley, U.S.A.

(*Received* 31 *January* 1994; *in revised form* 27 *April* 1994)

Abstract—The partial and complete perforation of woven carbon fiber/epoxy laminates with thicknesses ranging from 1.3 to 6.6 mm by 60° cylindro-conical hard steel strikers at normal incidence has been examined under both quasi-static and dynamic conditions. Quasi-static experiments were conducted in a standard testing machine at rates ranging from 0.012 to 6.5 s^{-1}, where the load–deflection was obtained. Ballistic tests employed a 12.7 mm diameter projectile with an aspect ratio of three fired from either a compressed gas or a powder gun at speeds varying from 30 to 310 m/s, with the initial and final velocity (when present) of the striker always measured, in addition to selected high-speed photographic recording. The damaged samples were carefully examined with respect to failure modes.

Major mechanisms of the deformation and damage processes were modelled on the basis of energy absorption, including global plate deflection, fiber breakage, delamination, formation and bending of petals, hole enlargement and friction between striker and sample. For the dynamic case, the predictions were 70–96% of the observed expenditure level. This is considered to be due to the absence in the analysis of factors such as inertia, strain-rate and wave propagation effects, matrix shearing and fragmentation, as well as obliquity and rotation motion of the striker. The correspondence in the case of static loading was considerably poorer, indicating substantial and non-measurable energy absorption by the test apparatus, including substantial frictional dissipation in the specimen holder and between sample and penetrator.

INTRODUCTION

Carbon fiber materials have one of the highest specific moduli among currently available composites, rendering them highly suitable for structural applications where deformations must be severely limited. On the other hand, these substances exhibit a relatively low damage tolerance to impact as gaged by their known low toughness values. Previous investigations of this material have included a low-velocity study of the delamination process under both local and line loading [see Choi and Chang (1991)] and impact of round-nosed strikers and steel spheres on thin carbon/epoxy plates up to 700 m/s [see Cantwell and Morton (1990)] producing perforation. However, no information had been obtained for the characteristics of such plates upon perforation by sharp pointed strikers. The purpose of this investigation is to determine the damage characteristics and corresponding impact properties under both static and dynamic conditions for this type of penetrator, using samples prepared in our laboratory.

The development of such a data base also permits a comparison of the performance of this laminate with that determined recently for a more ductile composite, polyaramid fiber/epoxy under similar methods of loading [see Zhu *et al.* (1992a, b)]. The investigation consisted of quasi-static loading at various rates and ballistic impact at various speeds from just below to well above the ballistic limit of three plate thicknesses. The corresponding analytical phase of the present study depends heavily on the approach delineated in these references.

SAMPLE FABRICATION

Plate specimens were fabricated using woven T-300/934 epoxy prepreg plies in a microprocessor-controlled heated platen press at 177°C and a pressure of 0.7 MPa for 2 hours. The fiber diameter was 9.2 μm and its modulus 210 GPa; the fiber volume fraction

† Current address: Ford Motor Co., Engineering Center, Dearborn, Michigan, U.S.A.

was 0.63. All plates had a quasi-isotropic lay-up $[0/+45/90]_{ns}$. Specimens were cut from the cured laminate into 120×100 mm with 45° edge cuts to fit the holder using a diamond blade to minimize edge damage. Upon employment of standard laminated plate theory and use of lamina data provided by the prepreg manufacturer†, the in-plane moduli E_x and E_y, as well as Poisson's ratio μ and the shear modulus G_{xy}, were computed to be

$$E_x = E_y = 53\,\text{GPa}\,(7.7 \times 10^6\,\text{psi})$$

$$\mu_{xy} = 0.3, \quad G_{xy} = 20.4\,\text{GPa}\,(2.95 \times 10^6\,\text{psi}).$$

EXPERIMENTAL ARRANGEMENT AND PROCEDURE

For all tests, specimens with thicknesses of 1.3, 2.5 and 6.6 mm were employed, corresponding to 4–20 plies.

(a) *Quasi-static tests*

This study was conducted on a Model TT-C 44.5 kN (10,000 lb) capacity Instron Universal Testing Machine with a maximum loading rate of 8.5 mm/s. The penetrator, identical to the projectile used in the ballistic tests, consisted of a 30 g, 12.7 mm diameter cylinder with a length of 38.1 mm, whose tip formed a 60° cone, that was loaded by the crosshead onto the sample through a special alignment fixture. Partial perforation was controlled by the use of a shim which stopped the manually operated crosshead at predetermined displacements. The load–displacement curve was obtained from a load cell located below the sample and the rotational motion of the screw. Subsequent to unloading, damaged plates were examined and photographed; selected samples were sectioned and optical micrographs were obtained. Some fine carbon fiber particles separated from the specimens and were found on the load cell.

(b) *Ballistic tests*

The dynamic experiments were performed using either a compressed nitrogen gun or a powder gun, both with a bore of 12.7 mm diameter, mounted on a massive steel support. The powder gun required employment of a 0.05 mm (2 mil) copper coating for the projectile to minimize barrel wear. The peak velocity of the gas gun for this striker was 200 m/s, whereas the corresponding initial velocity for the powder gun was 1000 m/s using IMR 4198 smokeless powder.

The initial velocity was determined by the interruption due to projectile passage of two laser beams spaced 152 mm apart located either near the muzzle end through two holes in the barrel or in front of the muzzle. The final velocity was ascertained by means of two sets of conducting screens. For a number of tests, the process was monitored by a Photec IV camera‡ illuminated by up to 1550 W of flood lighting. Synchronization of the camera operation is achieved by a delay circuit activated by the firing button with the setting determined by the approximate bullet velocity and the desired exposure at a point 70% along the film length. Further details and a schematic of the setup may be found in Zhu *et al.* (1992a).

Both the chamber pressure for the nitrogen gun and the amount of powder for the high-speed gun were ascertained from previous calibrations for the desired initial projectile velocity. In the former case, the striker was inserted in the barrel that arrested its forward motion by a pin; firing was achieved by withdrawal of this restraint by pneumatic action. For the powder gun, the projectile was inserted first and a shell with the required amount of powder was then placed directly behind and the breech was closed. Firing of this device was achieved in a closed, empty chamber by remote control.

† ICI, Tempe, Arizona, U.S.A.

‡ Photonic Systems, Sunnyvale, California; now Photographic Analysis Co., Wayne, New Jersey.

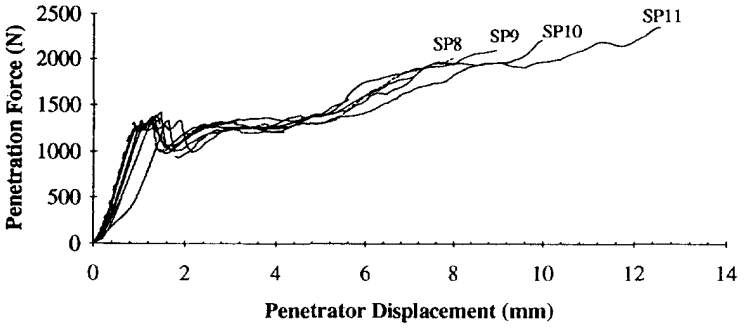

Fig. 1. Quasi-static perforation tests of 2.5 mm thick samples at a rate of 0.08 mm/s.

RESULTS

(a) *Quasi-static tests*

(*i*) *Partial perforation.* Eleven partial perforation tests of a 2.5 mm (0.1 in) thick specimen and complete perforation tests on samples of three thicknesses, 1.3 mm (0.05 in), 2.5 mm (0.1 in) and 6.6 mm (0.26 in), were conducted at a crosshead speed of 0.08 mm/s. One of the complete perforation experiments was duplicated to check repeatability. In addition, the 2.5 mm thick sample was subjected to three loading rates. The load–displacement data from the partial perforation tests are exhibited in Fig. 1. The perforation energies comprise the area under these curves up to maximum penetration; the results are presented in Table 1.

No damage is noted below a level of displacement of 0.76 mm which constitutes elastic plate deflection. The first observable permanent deformation occurs at the contact point at a displacement of 0.84 mm without any corresponding distal side damage. Additional loading usually produces four triangular distal side petals, with the cracks aligned along the fiber direction, starting at an indentation of 2.11 mm, as exemplified by Fig. 2. Occasionally, as indicated in Fig. 3, five petals are formed, with the extra crack aligned at 45° to the outside surface ply; this direction corresponds to the principal axes of the first ply below the exterior surface.

(*ii*) *Complete perforation.* Figure 4 portrays the force–displacement curve in a complete perforation test of a 2.5 mm thick sample at three loading rates. Figure 5 provides corresponding information for three sample thicknesses at the same loading rate of 0.08 mm/s. Petals are formed as in case (i), but an additional set of four petals corresponding to the 45° plies are formed upon perforation and consequent unloading of the sample. This feature is shown in Fig. 6. The energy to produce complete perforation of 2.5 mm thick samples at a penetration rate of 0.08 mm/s was found to be 22 J; it increases with loading rate for the same sample thickness, and increases almost quadratically with specimen thickness. This is

Table 1. Results of the partial perforation tests (conducted on 2.5 mm thick plates)

Test number	Penetrator displacement (mm)	Indentation force at end of test (N)	Indentation work (J)	Number of petals
SP1	0.762	565	0.01	0
SP2	0.838	934	0.32	0
SP3	2.108	1192	1.95	4
SP4	2.769	1312	2.77	4
SP5	4.166	1214	4.14	4
SP6	5.613	1116	6.28	4
SP7	7.137	1824	9.05	4
SP8	8.026	2006	10.77	4
SP9	8.992	2099	13	4
SP10	23.851	2211	14.65	4
SP11	12.573	2344	18.82	5

indicated in Table 2, which provides a summary of these tests. For the tests conducted, the peak force F is given by $F = -A + Bt$, where A and B are positive constants and t is the sample thickness, but, since extrapolation must result in a zero force value for a finite specimen thickness, this relation must become nonlinear as the origin is approached.

The load–deformation curves for partial and full penetration exhibit substantial similarities in an elastic deflection to a level just below 1500 N and a subsequent nearly linear region of rising load involving damage. For the perforation case, this region continues to the peak load and then suddenly drops to the level of frictional resistance which ranges from 62 to 890 N. The frictional resistance depends upon the shape of the crater, which is not always circular, and upon the elastic recovery of the plate upon load reduction. Greater amounts of fragmentation and detachment in the crater zone, indicating increased degrees of fracturing of the fibers, were noted with higher penetration speeds.

(b) *Dynamic tests*

Figures 7 and 8 depict sequences at 1000 frames/s of 2.5 mm samples struck by the projectile at and above the ballistic limit of 41 and 84.7 m/s, respectively. In all cases, the initial contact was at normal incidence, but in some cases the projectiles became yawed during perforation as the result of uneven loading on the projectile edge, possibly caused by local inhomogeneities. The results from the initial and terminal velocity measurements are presented in Tables 3–5 for the three sample thicknesses; the penetration energy is based upon these measurements.

In all ballistic tests, four petals were formed on the distal side of the sample. The damage pattern at the ballistic limit is shown in Fig. 9 for the 1.3 mm plate corresponding to an initial velocity of 29.9 m/s. Like all other craters, it consists of four petals which, for this case and for the thickest plate, both satin woven, remained attached. By contrast, the petals formed at the ballistic limit for the plate of intermediate thickness, which were plain woven, were essentially detached. The former are more likely to be less fragmented since, in satin weave, the fiber segment between intersections are longer and hence more compliant. This feature is also exhibited in data taken even above the ballistic limit, as indicated by the patterns exhibited in Fig. 10 for the plain weave and Fig. 11 for the satin weave.

The present tests, as well as previous investigations (Choi and Chang, 1992), indicate that, for cylindro-conical projectile perforation, the formation of the crater occurs in the form of a frustrum of a cone, with the smaller diameter located on the contact side. This is similar to the spallation phenomenon common in glasses and ceramics under conditions of impact.

(c) *Ballistic limit*

Figure 12 shows the variation of the ballistic limit as a function of plate thickness. As is also the case for metallic plates struck by cylindro-conical projectiles, used by Landkof and Goldsmith (1985), the curve is initially briefly concave downward, followed by a linear rise. The same pattern is observed for all three plate thicknesses when the exit velocity is related to the striking speed, as shown in Fig. 13. This type of relationship has been documented previously by an analytical model [see Landkof and Goldsmith (1985); Liss *et al.* (1983)]. The slopes of the linear regions in Fig. 13 are inversely proportional to the plate thickness.

PHENOMENOLOGICAL MODEL

The phenomenological representation of the event is based on an energy balance similar to that employed by Zhu *et al.* (1992a,b) for Kevlar composites subjected to corresponding perforation conditions; some of the parameters required an experimental evaluation. Good agreement had been obtained by Zhu *et al.* (1992a,b) between theoretical predictions and observations for Kevlar which involved global plate deflection, crack propagation, delamination, friction, fiber breakage, indentation and bulging. The last mechanism was not observed in the case of carbon fiber laminates, and hence was not considered here. Both fiber breakage and indentation occurred in a brittle manner at

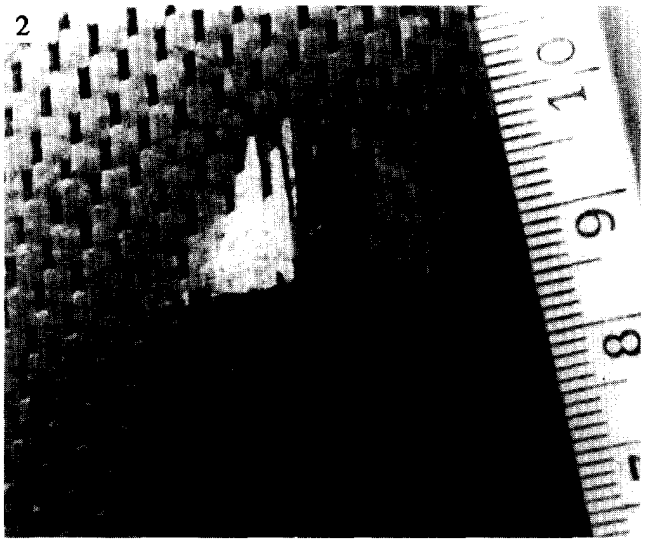

Fig. 2. Distal side petaling in quasi-static partial penetration of 2.5 mm thick samples.

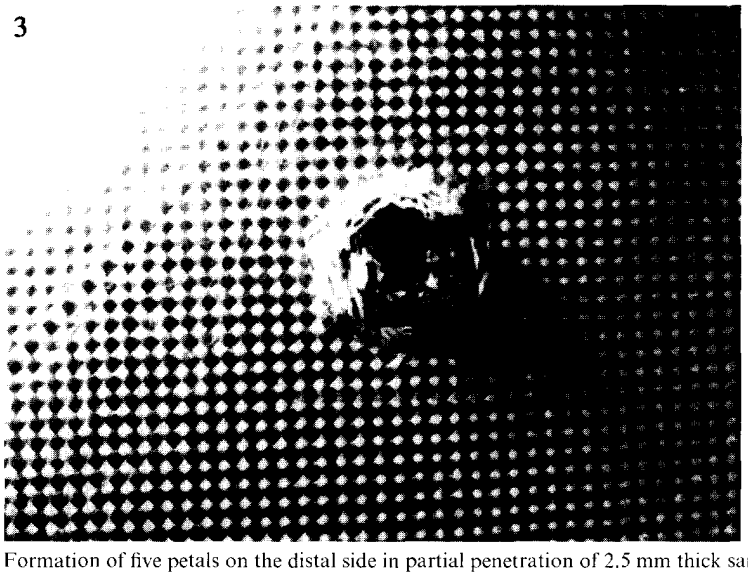

Fig. 3. Formation of five petals on the distal side in partial penetration of 2.5 mm thick samples.

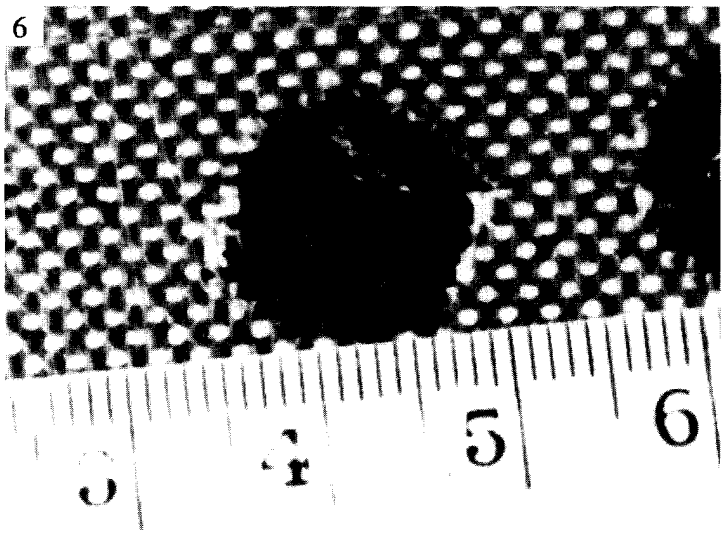

Fig. 6. Formation of eight petals on the distal side in complete perforation of a 2.5 mm thick sample.

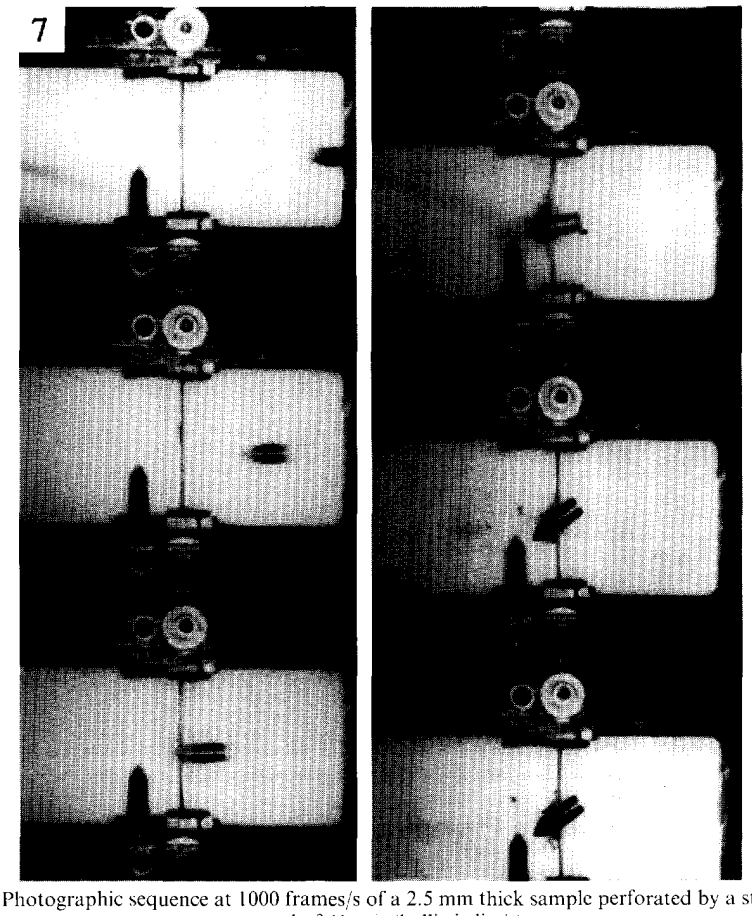

Fig. 7. Photographic sequence at 1000 frames/s of a 2.5 mm thick sample perforated by a striker at a speed of 41 m/s (ballistic limit).

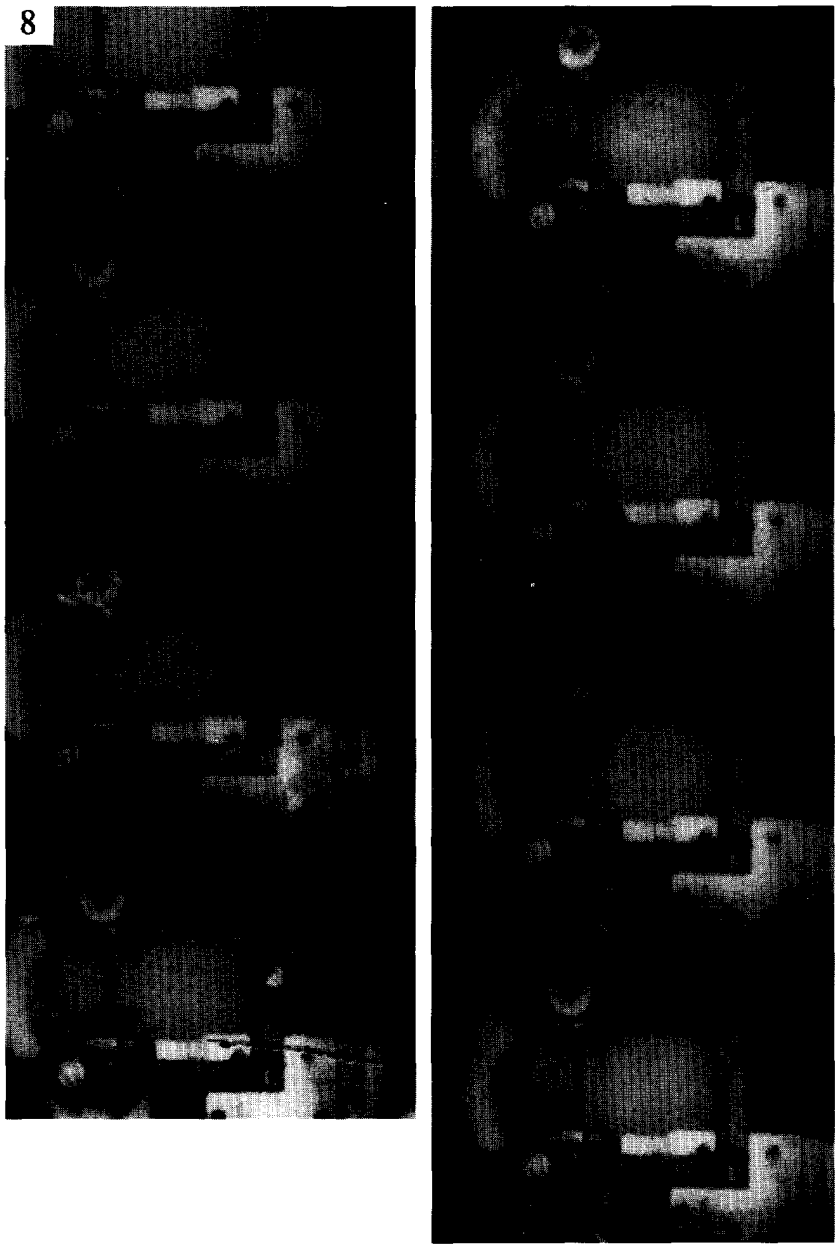

Fig. 8. Photographic sequence at 1000 frames/s of a 1.3 mm thick sample perforated by a striker at a speed of 84.7 m/s.

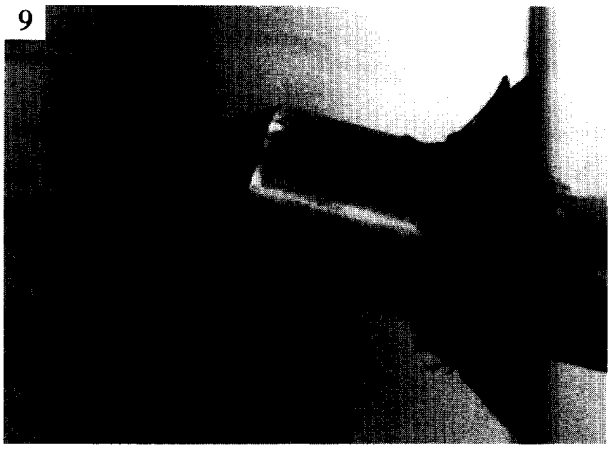

Fig. 9. Damage pattern for the 1.3 mm thick sample struck at a speed of 29.9 m/s (ballistic limit) showing four attached petals.

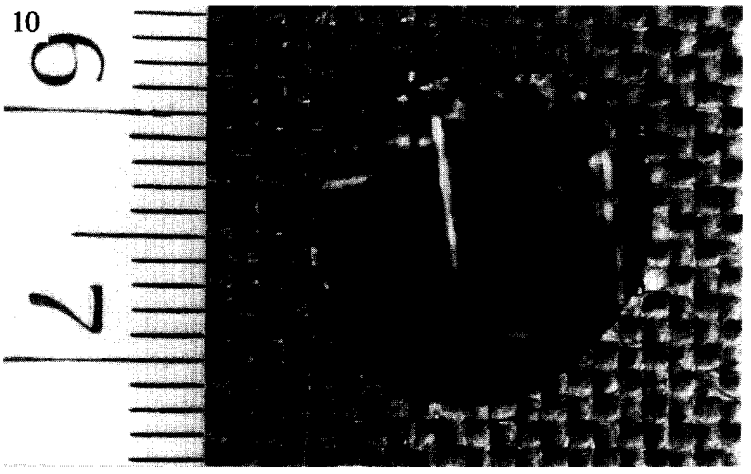

Fig. 10. Damage pattern for the 2.5 mm thick sample struck at a speed of 84.7 m/s showing detachment of petals.

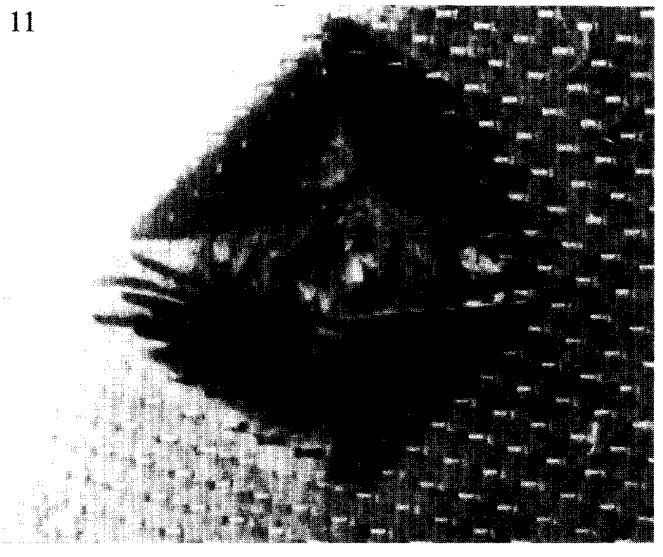

Fig. 11. Damage pattern for the 6.6 mm thick sample struck at a speed of 98.1 m/s showing attached petals.

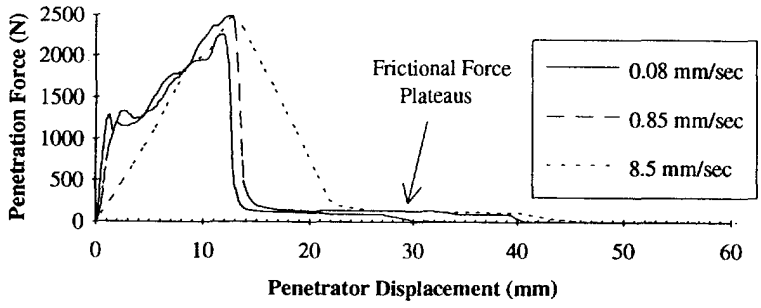

Fig. 4. Quasi-static perforation of 2.5 mm thick samples at different perforation speeds.

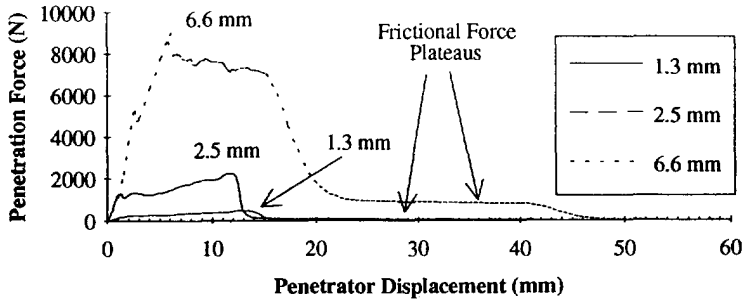

Fig. 5. Quasi-static perforation of samples of three thicknesses at a perforation speed of 0.08 mm/s.

Table 2. Results of complete penetration tests

Test number	Plate thickness (mm)	Total penetration energy (J)	Maximum penetration force (N)	Frictional force (N)	Hole diameter (mm)	Penetration speed (mm/s)
S1-2	2.5	22.2	2340	111	11.7	0.08
S1-3	2.5	21.6	2260	111	11.8	0.08
S1-4	2.5	25.6	2490	133	12.2	0.85
S1-5	2.5	32.4	2500	133	12.1	8.5
S2	6.6	140.5	9050	890	11	0.08
S3	1.3	6.33	490	62	11.4	0.08

Table 3. Results of impact test on 1.3 mm plates

Test number	Initial velocity (m/s)	Final velocity (m/s)	Penetration energy (J)
D3-1	71.4	66.7	9.4
D3-3	40.4	16.2	20
D3-4	29.9	0	13
D3-5	52.1	47.8	6.8
D3-6	107.8	107.3	1.5
D3-7	131.7	133.5	0
D3-8	93.3	93.1	0.3

Table 4. Results of impact tests on 2.5 mm plates

Test number	Initial velocity (m/s)	Final velocity (m/s)	Penetration energy (J)
D1-4	43	20.3	21.8
D1-6	33	0	16.5
D1-7	43.7	0	29
D1-8	44.3	0	29.7
D1-10	64.6	52	22.2
D1-11	78.3	60.4	37.8
D1-12	41	0	25.5
D1-13	84.7	59.8	54.5
D1-14	102.6	69.7	85.8

Table 5. Results of impact tests on 6.6 mm plates

Test number	Initial velocity (m/s)	Final velocity (m/s)	Penetration energy (J)
D2-1	81.7	0	101.2
D2-2	112.6	85.2	112.6
D2-3	136	90.4	149.5
D2-4	145	101	164.6
D2-5	108.6	80.8	76.4
D2-6	101.7	69	81.1
D2-7	98.1	63.2	85.1

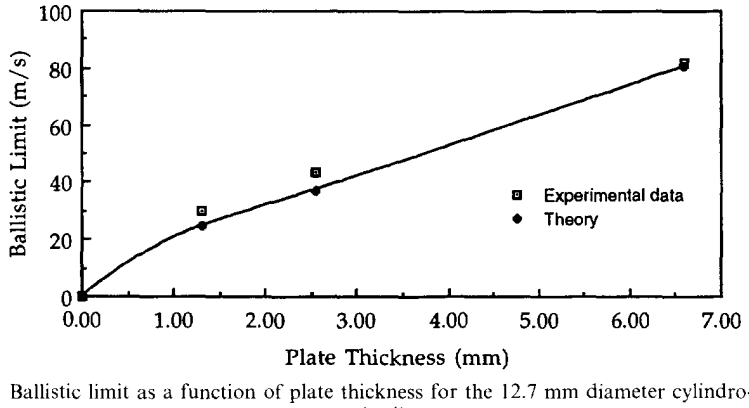

Fig. 12. Ballistic limit as a function of plate thickness for the 12.7 mm diameter cylindro-conical projectile.

relatively low strains and their effects were manifested differently, requiring an alternate modeling approach. An additional damage mode, petal bending, was prominently manifested and its energy component was treated as by Landkof and Goldsmith (1985).

The work done as the result of global plate deflection was obtained from the expression [see Roark and Young (1975)]

$$W_{\text{defl}} = [3F^2(1-\mu^2)(R^2-p^2)^2]/[8\pi ER^2t^3], \tag{1}$$

where F is the maximum force, taken here as the measured value from the quasi-static test, amounting to 490, 2400 and 9050 N for the 1.3, 2.5 and 6.6 mm thick plates. These values are considered to be the lower bound of the impact force, so that eqn (1) is very conservative. The quasi-isotropic laminate Poisson's ratio μ_{xy} and Young's modulus E ($= E_x = E_y$), previously cited, constitute the elastic constants of the system, R is the plate radius, t its thickness and p is the location of the applied load from the center of the plate. With an assumed value of $p = 0$ for all tests (even though this was not, in fact, always the case), the

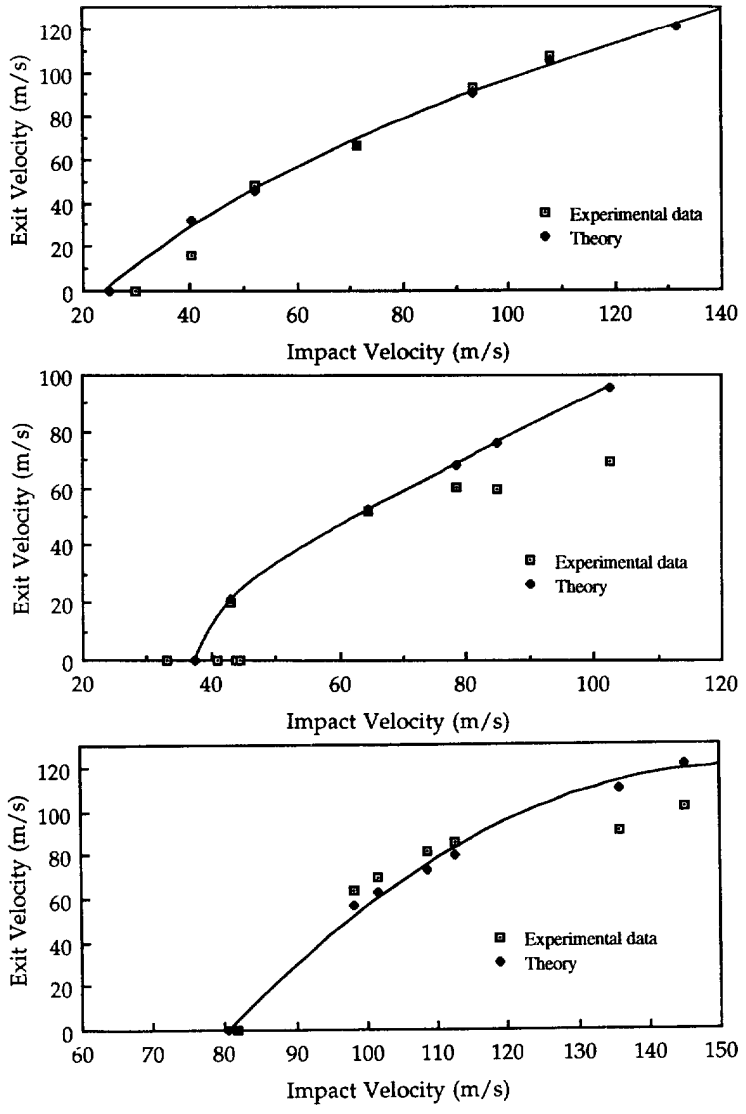

Fig. 13. Exit velocity as a function of initial velocity for the three sample thicknesses upon being struck normally by a 12.7 mm diameter cylindro-conical projectile.

values of the work of deflection do not increase monotonically with plate thickness due to the experimentally determined form of the force–thickness relation.

The compressive energy dissipated in the creation and relaxation of the conically shaped hole, observed both in the present tests and those of Cantwell and Morton (1990), was calculated by means of a linearly elastic model up to the yield stress, and is expressed by

$$W_{\text{comp}} = \pi a \sigma_y \delta_0 t_0, \tag{2}$$

where t_0 is the thickness of the conical edge of the crater that has been compressed, δ_0 is the shrinkage of the crater after passage of the projectile, both determined empirically, and $\sigma_y = 49$ MPa is the tensile yield stress for the matrix, taken from the literature. The value of δ_0 is obtained by subtracting the measured hole radius from the shank radius; the measured hole diameter is presented in Table 2. The compressed zone is small compared to the projectile diameter and $t_0 < t$ until compression extends to the impact surface;

Table 6. Summary of penetration energies

Plate thickness (mm)	1.3	2.5	6.6
Delamination energy (J)	0.2	1.6	2.6
Crack energy (J)	0.6	1.1	2.9
Energy to bend petals at ballistic limit (J)	0.5	1.9	17
Plate deflection energy (J)	0.9	3	2.3
Energy to overcome friction (J)	1.7	3.7	24.8
Energy to break fibers (J)	1.5	3	15
Energy to enlarge hole (J)	0.7	0.4	2.2
Theoretical static penetration energy (J)	5.6	12.9	49.9
Measured static penetration energy (J)	6.3	23.1	140
Ratio of predicted to measured static penetration energies	0.89	0.56	0.36
Theoretical dynamic penetration energy (J)	9.2	20.9	97
Measured dynamic penetration energy (J)	13	29	101
Ratio of predicted to measured dynamic penetration energies	0.7	0.72	0.96

Table 7. Predicted and measured ballistic limits

Plate thickness	Measured ballistic limit (m/s)	Predicted ballistic limit (m/s)
0.052 in (1.31 mm)	29.9	24.8
0.10 in (2.54 mm)	43.7	37.3
0.26 in (6.60 mm)	81.7	80.4

thereafter, $t_0 = t$. Furthermore, in view of the tip angle of 45°, $\delta_0 = t_0 = t$. Table 6 provides a summary of the computed components and measured total energy in both quasi-static and dynamic perforation.

The energy dissipated in fiber failure was obtained by utilizing a linear stress–strain curve with modulus $E_f = 210$ GPa up to the ultimate strain of 0.7% in the standard work expression. The number of failures was computed from the area of the hole, the number of fibers within the damage zone, and the observation that each fiber was broken three times, once at each edge of the hole and in the center, since the four petals produced separated from the remainder of the plate in all the present tests.

As was the case in the previous investigation (Zhu *et al.*, 1992b), the work of friction resulting from contact of the projectile shank with the crater is based on an experimentally determined friction force which was measured in quasi-static tests and found to be nearly constant for a given projectile diameter and plate thickness. The values for 1.3, 2.5 and 6.6 mm thick plates were found to be $F_f = 62$, 133 and 890 N, respectively. The frictional work is thus given by

$$Wk_f = F_f L_p, \tag{3}$$

where the length of the striker shank $L_p = 25.4$ mm.

DISCUSSION

Table 6 summarizes the component and total energies predicted from the various dissipation mechanisms considered in this analysis both on a quasi-static and dynamic basis. In the quasi-static calculation, failure is assumed to occur only once per fiber, while three such breaks were found in the dynamic tests, and these failure energies were adjusted accordingly.

The total energy absorbed in dynamic perforation is also presented in Table 7; the calculated fiber failure accounted for approximately half of this value. A comparison of the total predicted and measured energy loss indicates that the latter always exceeds the former, as is mandated in a reasonable model since some actual dissipative mechanisms, such as indentation of the specimen and vibratory effects, are neglected. For the limited data available, reasonably good correlation is obtained for the dynamic tests. For quasi-static

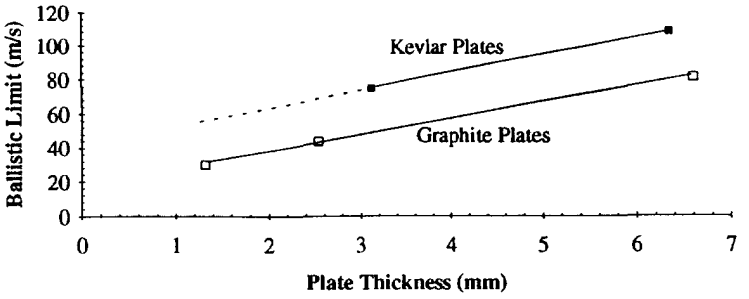

Fig. 14. Comparison of the ballistic limits of Kevlar and graphite laminates.

perforations, the agreement deteriorates substantially as the plate thickness is increased. A portion of this discrepancy may be attributed to the neglect of transverse shear deformation which becomes increasingly important with thickness and is not nearly as dominant in the dynamic case due to its rapid occurrence. Similarly, the work required to generate the indentation and concomitant local damage processes, such as fiber/matrix separation and plastic deformation, will increase as the thickness is augmented.

Table 7 presents the values of the calculated and measured ballistic limits for the three plates; the agreement is good. Figure 13 provides a similar comparison of the experimental and calculated values of the terminal velocity, the latter based on values of the perforation energy predicted by the model; the experimental energy loss can be determined from these results. The data exhibit slopes which decrease with increasing plate thickness. Agreement for the thinnest and thickest plates is very reasonable for the range investigated, with apparent increasing discrepancies for the 6.6 mm thick plate at higher velocities. Furthermore, this trend is exacerbated for the 2.5 mm thick plate. Thus, it appears as though the calculated work of perforation is significantly lower than what it should be, and additional mechanisms, some perhaps not apparent at this stage and perhaps nonlinear in the thickness (as is the case for global deformation), should be incorporated in the model to provide a more satisfactory correlation.

A comparison of the performance of the present striker with the sphere employed by Cantwell and Morton (1990) is complicated by the difference in the sizes, geometry and masses of the two projectiles as well as the structure of the target. Based solely on a ratio of the striker mass, the energy required for the penetration of a 1.3 mm thick specimen is ten-fold greater for the spherical geometry. This huge difference is attributed, to some degree, to the much more efficient cutting capability of the fibers in the case of the pointed striker, but is also affected in a quantitatively unknown manner by the nearly two-fold difference in diameter as well as the specimen lay-up. Comparison of the failure pattern indicates that, for comparable thicknesses of plate (2.5 mm), a conical crater is generated by both types of strikers, as noted previously. However, the delamination and fracture zone in the case of the spherical penetrator extends much further into the laminate than for the pointed striker, which is to be expected.

It is also useful to compare the ballistic response of the present material with another composite, Kevlar/epoxy, which has a lower density, but a higher strain to failure and a higher strength in tension. This substance, whose behavior is described in Zhu *et al.* (1992a), is compared on the basis of the observed ballistic limit and perforation energy (at this limit) in Figs 14 and 15. These results indicate that Kevlar is clearly superior in stopping sharp-pointed projectiles and hence absorbing more energy over the entire range of plate thicknesses investigated. This advantage is even more pronounced when the densities of these two materials, 1.29 and 1.58 g/cc, are taken into consideration. The nearly linear variation of the ballistic parameters for these two target materials as a function of aerial density is mirrored by data involving adjacent layers of ceramic, composite and metallic substances [see Mayseless *et al.* (1987)].

The failure characteristics for the graphite and Kevlar composites exhibit significant differences. The former showed virtually no delamination beyond the immediate vicinity of the cracked region, whereas the latter manifested such separation for a distance up to more

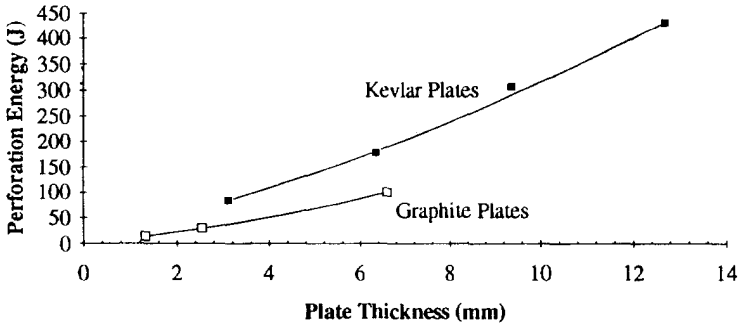

Fig. 15. Comparison of the observed perforation energy at the ballistic limit of Kevlar and graphite composites.

than four times the diameter of penetrator, primarily as the result of fiber stretching (Landkof and Goldsmith, 1985). Furthermore, graphite exhibited petaling instead of bulging in the contact area with no observable damage even slightly removed from the perforation. Since the graphite specimens were no more than half the maximum thickness of the Kevlar plates examined, it is not possible to ascertain definitively whether a thickening around the hole, strongly manifested in the Kevlar plates, would be generated in a corresponding graphite target. However, on the basis of the observed relatively brittle behavior of the carbon fiber composite, it is suspected that the pile-up around the crater would not occur with this material.

In addition to the mechanisms not considered in the model, but cited earlier, the analysis could be improved by a more general delamination/fracture characterization that includes mixed mode I and mode II fracture, as was actually observed on the distal specimen surface. It is believed that strain-rate and vibratory effects would not contribute significantly to the energy dissipation process.

CONCLUSIONS

An experimental and analytical investigation has been performed concerning the static and ballistic resistance of woven carbon fiber laminate plates with thicknesses up to 6.35 mm penetrated and perforated by a cylindro-conical projectile. It is concluded that:

(1) The very localized damage mechanisms manifested and included in the model of the process are crack propagation, fiber failure, petaling, delamination, hole enlargement and friction. Global deformation was also incorporated in the analysis.
(2) The measured static work of perforation is always less than the dynamic for the same specimen thickness.
(3) The ballistic limit increases approximately linearly over the range of thicknesses investigated. Correspondence with predicted values was uniformly satisfactory.
(4) Agreement between predicted and measured terminal velocities was quite reasonable for the thinnest and thickest plates, but deviated substantially for the plate of intermediate thickness, particularly at higher velocity. This trend is attributed to inaccuracies in the model for the damage process and to the neglect of mechanisms that contribute a significant component to the work of perforation and depend strongly on initial velocity.
(5) The perforation resistance of graphite plates of identical thickness is not nearly as good as those of Kevlar laminates, and the effectiveness is further diminished when the areal density of the two materials is considered.

Acknowledgments—A portion of this work was supported by the Air Force Office of Scientific Research under Contract AFOSR F49620-C-89-0127 and by a grant from the FMC Corporation.

REFERENCES

Cantwell, J. W. and Morton, J. (1990). Impact perforation of carbon fibre reinforced plastic. *Compos. Sci. Tech.* 38, 119–141.

Choi, H. Y. and Chang, F. K. (1991). Impact damage resistance of graphite/epoxy laminated composites. *Polymer Engng Sci.* **31,** 1294–1300.

Landkof, B. and Goldsmith, W. (1985). Petalling of thin, metallic plates during perforation by cylindro-conical projectiles. *Int. J. Solids Structures* **21,** 245–266.

Liss, J., Goldsmith, W. and Kelly, J. M. (1983). A phenomenological penetration model of the penetration of thin plates. *Int. J. Impact Engng* **1,** 321–341.

Mayseless, M., Goldsmith, W., Virostek, S. P. and Finnegan, S. A. (1987). Impact on ceramic targets. *J. Appl. Mech.* **54,** 373–378.

Roark, R. J. and Young, W. C. (1975). *Formulas for Stress and Strain*, 5th ed. McGraw-Hill, New York.

Zhu, G., Goldsmith W. and Dharan, C. K. H. (1992a). Penetration of laminated Kevlar by projectiles—I. Experimental investigation. *Int. J. Solids Structures* **29,** 399–420.

Zhu, G., Goldsmith, W. and Dharan, C. K. H. (1992b). Penetration of laminated Kevlar by projectiles—II. Analytical model. *Int. J. Solids Structures* **29,** 421–436.